Characteristic Length Scales of Reactive Species in a Convective Boundary Layer

HARM J. J. JONKER

Thermal and Fluids Sciences, Delft University of Technology, Delft, Netherlands

JORDI VILÀ-GUERAU DE ARELLANO

Meteorology and Air Quality Group, Wageningen University, Wageningen, Netherlands

PETER G. DUYNKERKE*

Institute of Marine and Atmospheric Research Utrecht, Utrecht University, Utrecht, Netherlands

(Manuscript received 6 January 2003, in final form 9 July 2003)

ABSTRACT

In this paper variance spectra of chemically active species in a dry convective boundary layer are studied by means of large-eddy simulations (LESs). The aim is to quantify the impact of chemistry on the spatial fluctuations in the concentration fields. The computational domain has a large aspect ratio (width/height = 16) in order to encompass all relevant scales (mesoscale to microscale). Variance spectra are used to calculate a characteristic length scale of the species' concentration variability. By locating the peak in the spectrum, a ''variance dominating length scale'' is derived.

For a simple first-order reaction, this length scale demonstrates a clear dependence on the reaction rate: an increase in the reaction rate leads to a significant decrease of the length scale of the species.

For a chemical cycle composed of a second-order reaction and first-order backreaction, the length scales turn out to depend much less on the reaction rate. The value of the length scales of the species involved appears to lie well in the mesoscale range, rather than the microscale range, demonstrating that concentration fluctuations are driven predominantly by scales much larger than the depth of the boundary layer.

External perturbation of the chemical balance can have a direct impact on the variance spectra. For the case where a (hypothetical) passing cloud switches off the chemical backreaction for a while, a dramatic drop in the length scale of the nonabundant species is observed. Once the feedback has been restored, a rapid increase of the length scale is observed.

To better understand these results, a spectral model is developed that incorporates turbulent production and dissipation of variance, chemistry, and spectral transfer. The model gives valuable insight into the relative importance of these processes at each scale separately, and enables one to predict the value of the variance dominating length scale in the limiting cases of very slow and very fast chemistry.

1. Introduction

Like any other atmospheric variable, chemical species are governed by a wide range of spatial and temporal scales. Some scales are much more pronounced than other scales, however, as can be observed by analyzing spectra. Variance spectra provide a decomposition of the total variance of a variable into contribution per time or length scale. One of the most interesting features of such spectra is the scale that contributes most to the variance, that is, the scale of the fluctuation that dominates the variance. Because this *variance dominating scale* is thought to carry the ''fingerprint'' of the underlying physical process that drives the fluctuations—for example, turbulence, waves, etc.—it provides much information on the process under study (Feijt and Jonker 2000).

This study analyzes the variance spectra of reactive species in the dry convective boundary layer (CBL) in order to establish how chemical transformations act upon spatial scales of the reactants. Pioneering theoretical research on turbulent reacting flows by Corrsin (1961) predicted changes in the spectra of reactants compared to inert species. More specific to the atmospheric case, our study is inspired by several observational studies (e.g., Lenschow et al. 1980; Delany et al. 1986; Pearson et al. 1998; Galmarini et al. 1999; Galmarini and Thunis 2000) that tend to reveal strong differences in the spectral behavior of reactants compared

* Deceased.

Corresponding author address: Dr. Harm J. J. Jonker, Thermal and Fluids Sciences, Faculty of Applied Sciences, Delft University of Technology, Lorentzweg 1, 2628 CJ Delft, Netherlands.
E-mail: h.jonker@ws.tn.tudelft.nl

to thermodynamic variables. In their study, which focused on ozone measurements taken from aircraft, Lenschow et al. (1980) found ozone to be dominated by significantly smaller length scales than the thermodynamical variables and suggested that these variations might be a result of chemical transformations. Delany et al. (1986) studied nitrogen and ozone fluxes over grassland and revealed important differences between, on the one hand, the cospectrum of vertical velocity (w) with ozone, and on the other hand, the cospectrum of w with NO (or NO_2). They also suggested that chemical transformations were responsible for altering the latter cospectra. Pearson et al. (1998) calculated ozone spectra from surface measurements over cotton and found similar behavior to the spectra of thermodynamic variables such as the temperature and moisture. In contrast, recent studies by Galmarini et al. (1999) and Galmarini and Thunis (2000) revealed striking differences between the spectra of chemically active species like nitrogen dioxide and ozone, and the spectra of vertical velocity and potential temperature: the chemical species were found to be dominated by fluctuations with a much larger horizontal scale (at least one order of magnitude) than vertical velocity and potential temperature.

It is difficult to fully understand these observations and to reconcile them. Clearly one has not enough data, but also the meteorological situation varies from case to case, as well as the measurement method (aircraft or ground based, etc.). In order to identify the underlying mechanism that drives the variability of reactive species, hypotheses need be checked and for this a variety of different situations would be needed. At this point controlled numerical simulations may be very helpful. They allow one to set up a ''clean'' case, to vary a single parameter at a time and study its impact. The present study employs large-eddy simulations (LESs) of the dry convective atmospheric boundary layer with chemically reacting species, comparable to the studies by, for example, Schumann (1989), Krol et al. (2000), Sykes et al. (1992), and Patton et al. (2001). The specific questions addressed in this paper are the following.

- Are the spectra of reacting species affected by chemical transformations?
- If so, what are the physical and chemical mechanisms responsible for the change, and to what degree are they dependent on, for example, the reaction rate and the reaction type?

As mentioned we will focus on a particular feature of the spectra: the horizontal scale that dominates the variance, or shortly, the variance dominating length scale. For boundary layer processes devoid of large-scale (mesoscale) forcings, one usually assumes this length scale to be roughly equal to the depth of the boundary layer—typically 1 km. It is assumed to be the same for all dynamic variables, that is, for the thermodynamic variables, temperature and moisture, as well as for momentum. However, for buoyancy-driven clear and cloudy boundary layers, the picture has turned out to be more complicated. Both experimental studies (e.g., Young 1987; Nucciarone and Young 1991) and numerical studies (e.g., Fiedler 1993; Fiedler and Khairoutdinov 1994; Müller and Chlond 1996; Shao and Randall 1996; Dörnbrack 1997; Jonker et al. 1999) have shown that generally a significant amount of variance is present at mesoscales for quantities such as moisture, temperature, and the horizontal wind components; only the length scale of vertical velocity is consistently found to be on the order of the boundary layer depth [for a recent discussion see de Roode et al. (2004)]. This shows that even for the nonreacting case, the length-scale issue is not entirely clear at present.

As a starting point for a numerical study into the reacting case, we took the LES study by Jonker et al. (1999) because of its apparent simplicity. They studied a dry convective boundary layer in the absence of large-scale forcings, and analyzed the spectra of both (thermodynamic) variables and passive (inert) scalars. Even for this elementary nonreacting case, a striking disparity in the horizontal length scales of different variables was observed: the length scale of inert species tended to grow as large as the domain size, while at the same time, the length scale of both vertical velocity and potential temperature remained equal to the boundary layer depth. In our study, we extend this analysis by studying, under similar conditions, the length scales of reacting species. We start by analyzing a first-order chemical reaction (decaying species) for varying reaction rates (section 3). In section 4 we turn to the more complicated case of a chemical cycle, where chemical balance can be reached due to a backreaction. We also study the effect of disturbing this chemical equilibrium on the species' length scales, by temporarily switching off the chemical backreaction. To better understand the observed results, we develop in section 5 a conceptual model that incorporates multiple scales, chemistry, turbulent production and dissipation of variance, and a simple parameterization of the interaction between scales. Conclusions are presented in section 6.

2. Fluctuations in concentrations of reactive species

a. Governing equations

The generic chemical system under study comprises three species (a, b, and c), which react as follows:

$$a + b \xrightarrow{k} c, \tag{1}$$

$$c \xrightarrow{j} a + b, \tag{2}$$

where k and j are second- and first-order chemical constant rates, respectively. The chemical system (1), (2) is inspired on the atmospheric cycle $NO + O_3 \leftrightarrow NO_2$. Departures from the equilibrium of this system (Calvert and Stockwell 1983) due to atmospheric phenomena or exchange mechanisms of the reactants can have a direct

impact on ozone production. For instance, the reaction rate j, which represents the photodissociation rate, is a function of the ultraviolet radiation level (Madronich 1987) and can thus be perturbed, for example, by the presence of clouds.

Denoting the concentration field of the reactants by $s_\alpha (=a, b, c)$, and performing a Reynolds decomposition into an ensemble mean $S_\alpha = \overline{s_\alpha}$ and deviations from it $s'_\alpha = s_\alpha - S_\alpha$, one obtains the following equation governing the average concentration of the reactants:

$$\frac{\partial S_\alpha}{\partial t} + U_i \frac{\partial S_\alpha}{\partial x_i} = -\frac{\partial \overline{u'_i s'_\alpha}}{\partial x_i} + R_{S_\alpha}, \tag{3}$$

where U_i represents by Reynolds-averaged wind velocity and u'_i deviations from U_i. The chemical term is R_{S_α}. For the different species, it reads

$$R_A = R_B = -k(AB + \overline{a'b'}) + jC,$$
$$R_C = k(AB + \overline{a'b'}) - jC.$$

The description of the concentration fluctuations both in space and time is important for two reasons: it provides information regarding the variability in the concentration fields and, for the reactants, it describes how the turbulent mixing state controls the chemical transformation. The governing equation for the covariance between two different chemical species is

$$\frac{\partial \overline{s'_\alpha s'_\beta}}{\partial t} + U_i \frac{\partial \overline{s'_\alpha s'_\beta}}{\partial x_i} = -\overline{u'_i s'_\alpha}\frac{\partial S_\beta}{\partial x_i} - \overline{u'_i s'_\beta}\frac{\partial S_\alpha}{\partial x_i} - \frac{\partial \overline{u'_i s'_\alpha s'_\beta}}{\partial x_i} - (D_\alpha + D_\beta)\overline{\frac{\partial s'_\alpha}{\partial x_i}\frac{\partial s'_\beta}{\partial x_i}} + R_{\overline{s'_\alpha s'_\beta}}, \tag{4}$$

where D_α and D_β are the molecular diffusivities for species α and β. The variance equation is a special case of (4):

$$\frac{\partial \overline{s'^2_\alpha}}{\partial t} + U_i \frac{\partial \overline{s'^2_\alpha}}{\partial x_i} = -2\overline{u'_i s'_\alpha}\frac{\partial S_\alpha}{\partial x_i} - \frac{\partial \overline{u'_i s'^2_\alpha}}{\partial x_i} - 2D_\alpha \overline{\frac{\partial s'_\alpha}{\partial x_i}\frac{\partial s'_\alpha}{\partial x_i}} + R_{\overline{s'^2_\alpha}}. \tag{5}$$

The physical interpretation of the terms on the right-hand side of the variance equation (5) is as follows: production of variance governed by the mean gradient concentration, turbulent transport of variance, dissipation of variance due to molecular diffusion, and variance changes due to chemistry (R). Note that transport due to molecular diffusion has been neglected in (3) through (5).

A scale-by-scale interpretation of (5) is one where the production term creates variance on a large scale, from where it is transferred to smaller scales by nonlinear interaction (the cascade), until it dissipates at the smallest scales. A priori, the effect of chemistry in this process is unclear.

TABLE 1. Initial and boundary conditions of the turbulent reacting flow in the boundary layer simulation.

Domain size	12.8 km × 12.8 km × 1250 m
Grid	128 × 128 × 50
Initial boundary layer depth	750 m
Initial inversion strength	7 K
Surface heat flux	30 W m^{-2}

b. Large-eddy simulations

The turbulent reacting flow is simulated using an LES code developed by Cuijpers and Duynkerke (1993) with later modifications to the scalar advection scheme (Vreugdenhil and Koren 1993). The chemical solver is based on an analytical solution of the reactant governing equations (see section 4 and appendix A). Table 1 shows the prescribed initial and boundary conditions. The dynamic characteristics of the CBL are the same as those obtained by Jonker et al. (1999). Large-scale forcings are not included; in particular, no Coriolis forcing and no pressure gradient was applied. The convective velocity scale is $w_* = 0.86$ m s^{-1}, and the large eddy turnover time is $t_* = z_i/w_* \approx 900$ s. The total integration time is 10 h ($40t_*$). During this period, the height of the boundary layer rises to approximately 800 m.

In section 3 we study a first-order reaction, and in section 4 we study chemistry in equilibrium. Note that in all cases there is no feedback of chemistry onto the dynamics. This implies that in each of the cases the dynamics are similar. This aspect greatly facilitates comparison of the results between the various cases.

3. First-order reactions

We begin by analyzing the relatively simple case of a first-order reaction. In (1) and (2), we set the second-order reaction rate k to zero, so that species c decays according to

$$\frac{\partial c}{\partial t} = -jc.$$

For a horizontally homogeneous boundary layer with no mean wind, the governing equations (3) and (5) for mean concentration and variance become

$$\frac{\partial C}{\partial t} = -\frac{\partial \overline{w'c'}}{\partial z} - jC \quad \text{and} \tag{6}$$

$$\frac{1}{2}\frac{\partial \overline{c'^2}}{\partial t} = -\overline{w'c'}\frac{\partial C}{\partial z} - \frac{1}{2}\frac{\partial \overline{w'c'^2}}{\partial z} - D_c\overline{\left(\frac{\partial c'}{\partial x_i}\right)^2} - j\overline{c'^2}. \tag{7}$$

Compared to a nonreacting passive scalar, the extra contribution to the variance budget is the chemical term $R_{\overline{c'c'}} = -j\overline{c'^2}$. It is immediately clear that for the first-order reaction the chemistry can only reduce variance. Similar to the dissipation term, the chemical term is negative definite, but there is an important difference: due to the spatial derivatives, dissipation is most effec-

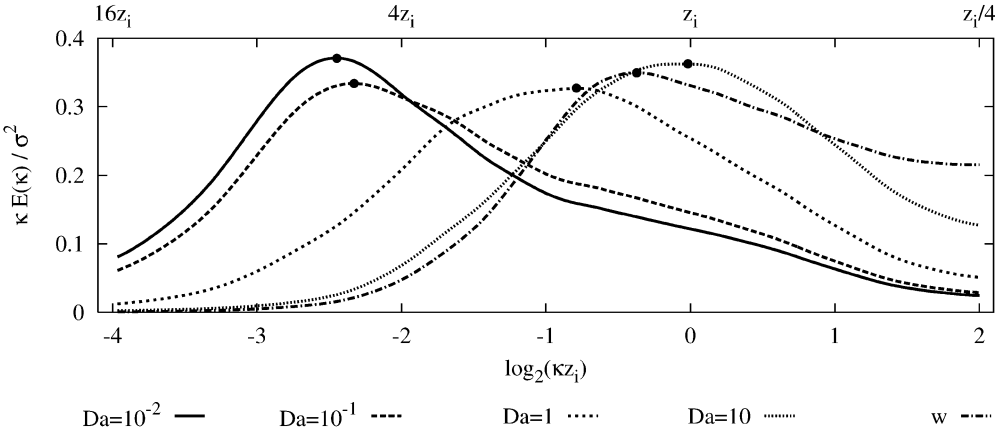

FIG. 1. Variance spectra of chemical species for various Damköhler numbers Da = jt_* at $t = 40t_*$. The spectra are plotted on log-linear axes, and normalized by the variance. In this way the area under each curve amounts to unity. The solid dots indicate the location of the spectral peaks κ_{peak}, which yield the corresponding dominating length scale Λ (cf. Fig. 2b). As a reference, the normalized variance spectrum of w has been plotted.

tive at small scales, but the chemical term can be equally effective on all scales.

To study the impact of the reaction rate j on the concentration fluctuations c', in particular on the spatial scales, we analyze the (spatial) variance spectrum $E_c(\kappa)$ for various values of j. In each case the surface flux of c is $\varphi_c = 0.1$ ppb m s^{-1}, and the initial concentration of c is zero. The precise definition of the variance spectrum $E_c(\kappa)$ is given in appendix B. It is based on the two-dimensional Fourier transform of c' and provides a decomposition of the variance according to

$$\overline{c'^2} = \int_0^\infty E_c(\kappa)\, d\kappa. \tag{8}$$

Like the variance $\overline{c'^2}$ itself, the variance spectrum is still a function of time t and height z; that is, $E_c(\kappa) = E_c(\kappa, z, t)$. We confine ourselves to instantaneous spectra taken at $t = 10$ h ($\approx 40t_*$) in the middle of the planetary boundary layer (PBL) $z = z_i/2$. A useful dimensionless number for describing the relationship between the time scale of turbulence and the time scale of the chemical transformation is the Damköhler number, which is defined as Da = t_*/τ_c, where τ_c is the characteristic time scale for the reaction, and $t_* = z_i/w_*$ the time scale for turbulence in a CBL ($t_* = 900$ s in the present case). For a first-order reaction, we simply have Da = jt_*. In Fig. 1 we show the resulting spectra for Damköhler numbers ranging from Da = 10^{-2} to Da = 10^{+1}. The spectra are plotted in the variance conserving form; that is, they have been multiplied by κ to compensate for the logarithmic κ axis, since $E(\kappa)d\kappa = \kappa E(\kappa)d\log(\kappa)$. In addition we have normalized the spectra by the total variance $\sigma^2 = \overline{c'^2}$ in each case, because we are interested in the distribution of variance over the spatial scales, rather than in the actual value of the variance. By virtue of (8), this normalization implies that the area under all curves amounts to unity. To facilitate comparison, the spectra have been additionally smoothed (Press et al. 1992, p. 650ff). As a reference we have included the normalized variance spectrum of the vertical velocity.

Figure 1 reveals a clear impact of the reaction rate j on the spatial scales of the concentration fluctuations. For small values of Da the variance is dominated by horizontal scales much larger than PBL depth z_i. This is in accordance with the results of Jonker et al. (1999), who reported similar findings for inert passive scalars (Da = 0). Comparison with the variance spectrum of vertical velocity $E_w(\kappa)$ reveals the remarkable aspect that the species fluctuations are dominated by much larger scales than the dynamics. The spectrum of w peaks at $1/\kappa_{peak} \approx z_i$ as one would expect in a dry CBL (e.g., Garratt 1992; Stull 1988), whereas for small values of Da, the variance spectra $E_c(\kappa)$ peak at $1/\kappa_{peak} > 5z_i$. The contribution of large scales to the variance is still growing; that is, if one extends the simulation period, the peak will shift to even larger scales. However, for higher values of the reaction rate j, that is, higher Damköhler numbers, the large-scale fluctuations get suppressed progressively, and the spectral peak shifts to smaller scales (higher wavenumbers). At Da = 10^{+1} the peak is $1/\kappa_{peak} \approx z_i$, similar to w. Damköhler numbers larger than 10 could not be faithfully simulated with the present resolution, since the mean concentration gradient near the surface becomes too steep.

To show the influence of Da more directly, we will study the effect on the location of the spectral peak. To this end we introduce the length Λ defined as

$$\Lambda \equiv 1/\kappa_{peak}.$$

Because the spectral contribution to the variance is maximum at this scale, we will refer to Λ as the ''variance dominating scale.'' In Fig. 2a we plot Λ/z_i as a function of dimensionless time t/t_* for various Damköhler numbers. One observes that for small reaction rates the con-

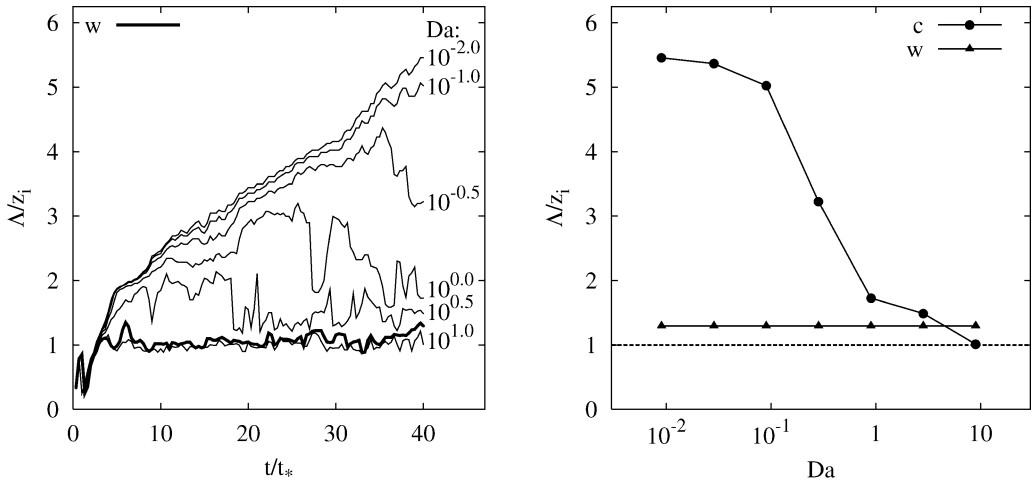

FIG. 2. (a) Variance dominating length scale Λ of first-order reacting species as a function of dimensionless time for different reaction rates (Damköhler numbers). For small Da the contribution of large scales to the variance is still increasing. (b) Variance dominating length scale at $t = 40t_*$ as a function of the Damköhler number. The graph reveals the strong dependence of spatial fluctuations of reacting species on the reaction rate. As a reference, the variance dominating length scale of vertical velocity has been plotted.

tribution of large-scale fluctuations to the variance is still growing. For Da $= O(1)$ and larger, the spectra appear to have reached a (statistically) stationary state. Actually, after close inspection of Fig. 2a, one might speculate that each curve shows a marked point in time after which the variance dominating scale no longer increases. This point in time depends on the Damköhler number: the smaller the Damköhler number, the longer it takes before Λ ceases to grow. For Da $\leq 10^{-1}$, the simulation period is too short to observe saturation of Λ.

Figure 2b shows Λ/z_i as a function of the Damköhler number Da at $t = 40t_*$. The graph reveals in a dimensionless form how spatial scales depend on temporal scales and conveys the main message of this section. The spatial fluctuations of first-order reacting chemical species in a convective atmospheric boundary layer are strongly dependent on the reaction rate. In the next section we will show that not only the reaction rate plays a significant role, but also the reaction type.

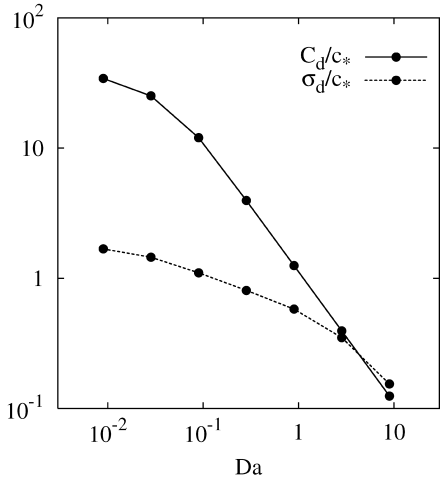

FIG. 3. Domain-averaged mean C_d and rms fluctuations σ_d of the concentration field as a function of the Damköhler number. The data have been normalized by the concentration scale c_*.

Finally, in order to provide some indication of the magnitude of the variance for different Damköhler numbers, we have calculated the domain-averaged variance $\sigma_d^2 = z_i^{-1} \int_0^{z_i} \overline{c'^2}\, dz$, and for comparison, the domain-averaged concentration $C_d = z_i^{-1} \int_0^{z_i} C(z)\, dz$. The results at $t = 40t_*$, presented in Fig. 3, have been normalized by the concentration scale $c_* = \varphi_c/w_*$, where φ_c is the surface flux. The mean follows a Da^{-1} dependence, which is to be expected from (6). Integrating over z_i and dividing by $c_* z_i$ yields

$$\frac{d}{dt}\frac{C_d}{c_*} = \frac{\mathrm{Da}}{t_*}\left(\mathrm{Da}^{-1} - \frac{C_d}{c_*}\right). \tag{9}$$

This equation also reveals that the time scale for C_d to reach a steady state amounts to t_*/Da and explains why for small Da the results are not yet equilibrated. It is furthermore interesting to observe that the ratio σ_d/C_d increases for increasing Da.

4. Chemistry in and out of equilibrium

a. Case description and chemical solver

We now turn to the generic chemical system (1), (2), that is, with k no longer zero. The combination of a forward reaction and a backreaction brings a new relevant feature into play: chemical balance.

As mentioned, the chemical system $a + b \leftrightarrow c$ we study is inspired by the atmospheric reaction $NO + O_3 \leftrightarrow NO_2$; Table 2 shows the initial conditions and the value of the (uniform) surface fluxes of species *a*, *b*, *c*

TABLE 2. Reaction rates, initial conditions, and boundary conditions with regard to the species involved in the reaction $a + b \leftrightarrow c$.

	Value	Unit
Concentration A ($z \leq z_i$)	1	ppb
Concentration B ($z \leq z_i$)	20	ppb
Concentration C ($z \leq z_i$)	2	ppb
ΔA (z_i)	0	ppb
ΔB (z_i)	10	ppb
ΔC (z_i)	0	ppb
Surface flux a	0.1	ppb m s^{-1}
Surface flux b	0.0	ppb m s^{-1}
Surface flux c	0.05	ppb m s^{-1}
Reaction rate j	10^{-3}	s^{-1}
Reaction rate k	10^{-4}	(ppb s)$^{-1}$

with the identification $a = [NO]$, $b = [O_3]$, $c = [NO_2]$; the profiles and reaction rates are based on realistic values (e.g., Vilà-Guerau de Arellano et al. 1990; Brown and Bilger 1996; Krol et al. 2000; Lewellen and Lewellen 2001). Ozone deposition fluxes, which could be relevant in realistic situations, have been ignored in this study. Rather than confining ourselves to the reaction rates j and k reported in Table 2, we study a much larger range of values of j and k to obtain a more comprehensive picture.

In the mixed-layer, the system is at $t = 0$ exactly in chemical balance, the so-called photostationary state

$$kAB = jC. \tag{10}$$

At $t = 0$ convection is initiated, causing concentration fluctuations due to the surface fluxes of a and c, and due to entrainment of species b. The magnitude of the entrainment flux that develops is $|\overline{w'b'}(z_i)| = 0.01 - 0.02$ ppb m s^{-1}. The dynamics is exactly similar to the previous case of the first-order reaction; see Table 1.

The chemical solver used in the LES model is based on the analytical solution of the reaction system (1), (2). The nonlinear equation system can be written

$$\frac{\partial a}{\partial t} = \frac{\partial b}{\partial t} = -kab + jc, \qquad \frac{\partial c}{\partial t} = kab - jc. \tag{11}$$

In the LES, the chemistry is treated by assuming that the species are homogeneously mixed at scales smaller than the grid size. After the resolved turbulent and subgrid transport have been calculated for every grid box and the concentrations have been updated accordingly, chemistry takes place during a period of Δt (the computational time step) in every grid box, taking the newly updated values of $a(t)$, $b(t)$, $c(t)$ as initial condition. Fortunately, a general analytical solution for this reaction could be derived (see appendix A), which is a generalization of Corrsin's solution for a binary reaction (Corrsin 1968). The analytical solution (A4)–(A6) enabled us to obviate usage of an iterative chemical solver, which would have been computationally much more expensive. The computation time saved in this manner could in turn be invested in resolving a large range of scales simultaneously, that is, a large domain size, necessary for resolving at least part of the mesoscale, while keeping the grid spacing at an acceptable small size for resolving turbulent eddies.

We carried out six simulations where we varied the reaction rates k and j. The reaction rates k were varied from $k = 10^{-7}$ to 10^{-2} (ppb s)$^{-1}$ by factors of 10, while keeping the ratio $j/k = 10$ ppb fixed. It should be noted that the results presented below depend on the specific choice $j/k = 10$. We do not perform a systematic study of other ratios j/k.

In Fig. 4a we show the mean profiles after 5 h (averaged over 1 h) for the case where $k = 10^{-4}$ (ppb s)$^{-1}$, $j = 10^{-3}$ s^{-1}. Figure 4b shows the turbulent fluxes $\overline{w'a'}$, $\overline{w'b'}$, $\overline{w'c'}$ at $t = 5$ h, also averaged over 1 h. The symbols indicate the fluxes for the reaction rates $k = 10^{-4}$ (ppb s)$^{-1}$, $j = 10^{-3}$ s^{-1}. As a reference, we present in the same plot the fluxes for the virtually non-

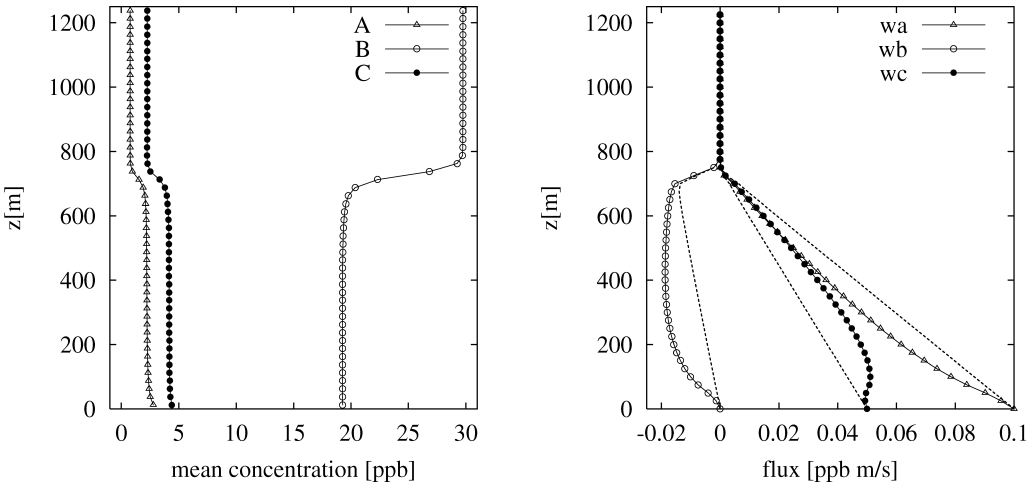

FIG. 4. (a) Mean vertical concentration profiles at $t = 5$ h ($=20t_*$) for the reaction rates $k = 10^{-4}$ (ppb s)$^{-1}$, $j = 10^{-3}$ s^{-1}. (b) Corresponding vertical flux profiles; as a reference, the dashed lines indicate the flux profiles for the nearly nonreacting case $k = 10^{-7}$ (ppb s)$^{-1}$, $j = 10^{-6}$ s^{-1}, demonstrating the effect of chemistry.

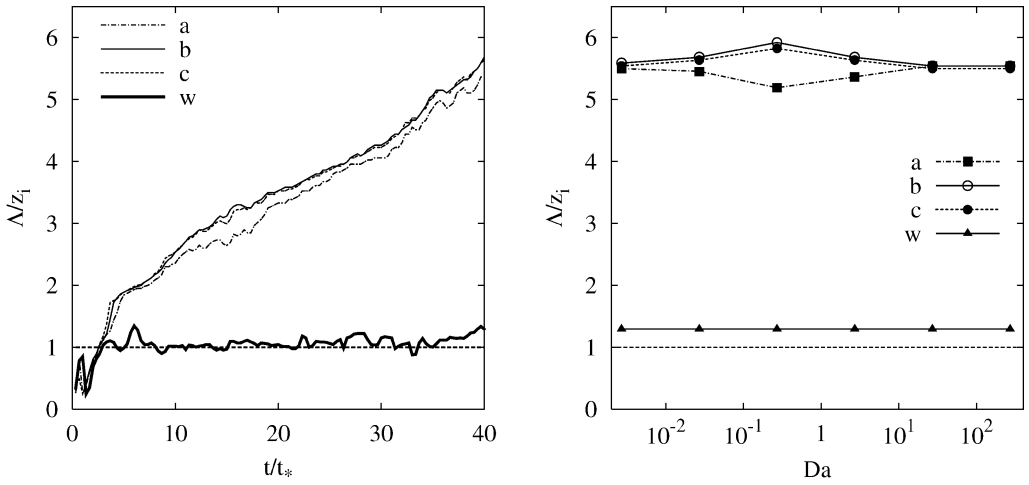

FIG. 5. (a) Variance dominating length scale of species *a*, *b*, and *c* as a function of time; The reaction rates are $k = 10^{-4}$ (ppb s)$^{-1}$, $j = 10^{-3}$ s^{-1}, corresponding to a Damköhler number of Da = 2.7. (b) Variance dominating length scales as a function of the Damköhler number Da $= t_*/\tau_{\text{chem}}$ at $t = 10$ h $= 40t_*$.

reacting case of $k = 10^{-7}$, $j = 10^{-6}$ (dashed lines). For these reaction rates the species can be regarded more or less as inert passive scalars, and the flux profiles exhibit a linear dependence on height as expected from quasi stationarity. The differences between the flux profiles (symbols versus dashed line) reveal the effect of chemistry (see, e.g., also Gao and Wesley 1994; Vinuesa and Vilà-Guerau de Arellano 2003).

b. Effect of chemistry on length scales

In this section we study the effect of increasing reaction rates on the variance dominating length scales of the species. Similar to the first-order reaction we calculated variance spectra of the concentration fields *a*, *b*, *c*, which decompose the corresponding variances:

$$\overline{a'^2} = \int_0^\infty E_a(\kappa)\, d\kappa, \qquad \overline{b'^2} = \int_0^\infty E_b(\kappa)\, d\kappa,$$

$$\overline{c'^2} = \int_0^\infty E_c(\kappa)\, d\kappa. \tag{12}$$

Recall that both spectra and variances are functions of time *t* and height *z*. Again we confine ourselves to instantaneous spectra in the middle of the PBL $z = z_i/2$. Based on these spectra, we determined the variance dominating length scales $\Lambda_a(t)$, $\Lambda_b(t)$, $\Lambda_c(t)$ by locating the spectral peak in each spectrum (see section 3):

$$\Lambda_a = 1/\kappa^a_{\text{peak}}, \qquad \Lambda_b = 1/\kappa^b_{\text{peak}}, \qquad \Lambda_c = 1/\kappa^c_{\text{peak}}.$$

In Fig. 5a, we show the development of the variance dominating length scales in time for the case where $k = 10^{-4}$ (ppb s)$^{-1}$ and $j = 10^{-3}$ s^{-1}. The figure reveals the steady growth of Λ for all three variables. As a reference we have plotted Λ_w.

In order to show the influence of the chemical reaction rates on the length scales, which was so manifest for the first-order reaction (Fig. 2b), we first have to define an appropriate Damköhler number. The time scale of the chemical reaction can easily be extracted from the analytical solution given in appendix A [see (A10)]. Because species *b* is largely in excess, this chemistry time scale can be simplified to $\tau_{\text{chem}} = 1/(kB + j)$, yielding an overall Damköhler defined by

$$\text{Da} \equiv \frac{t_*}{\tau_{\text{chem}}} = (kB + j)t_*. \tag{13}$$

Because we keep the ratio $j/k = 10$ ppb fixed in all runs, and $B = 20$ ppb, the expression for the Damköhler number becomes Da $= 30kt_*$. Since *k* ranges from 10^{-7} to 10^{-2}, and $t_* = 900$ s, the Damköhler number ranges (roughly) from $10^{-2.5}$ to $10^{+2.5}$.

In Fig. 5b we show the variance dominating length scales at $t = 10$ h $= 40t_*$ as a function of the Damköhler number. The difference with the first-order chemistry (Fig. 2b) is striking, because there is hardly any dependence on the Damköhler number in Fig. 5b. Especially for large values of Da, the fast chemistry limit, the situation is entirely different from the first-order reaction and, in fact, rather counterintuitive.

The results can be understood, however, by taking a closer look at the governing equations for the fluctuations. For the first-order reaction the chemical effect on the fluctuations is

$$\frac{\partial c'}{\partial t} = -jc', \tag{14}$$

which shows that chemistry acts to destroy the fluctuations. Turbulence, on the other hand, generates concentration fluctuations. The two processes are thus counteracting, and the balance that arises between the two processes, will critically depend on the relative strength

of the processes. One therefore anticipates a strong dependence on the Damköhler number, which is defined to embody the relative importance of turbulence versus chemistry.

In the case of the backreaction, a possibility arises where chemistry and turbulence are not counteracting. Focusing again on the fluctuations due to chemistry, we derive from (11)

$$\frac{\partial}{\partial t}a' = \frac{\partial}{\partial t}b' = -\frac{\partial}{\partial t}c' = -k(Ab' + Ba') + jc' + \text{turbulent transport.} \quad (15)$$

Higher-order terms have been neglected in (15) because $|a'| \ll A$, $|b'| \ll B$, which can be concluded from the concentration scales $a_* = \overline{w'a'}(0)/w_*$ and $b_* = -\overline{w'b'}(z_i)/w_*$. In the LES we find typically $\overline{a'b'}/(AB) \simeq -5 \times 10^{-4}$ for the different Da.

In the case of fast chemistry (Da $\gg 1$) the fluctuations will be completely ruled by the chemistry part of (15), because the effect of turbulence is of marginal importance, driving the system into the stationary state

$$Ab' + Ba' = \frac{j}{k}c' \quad (16)$$

at each spatial location. Similar to the mean concentrations in (10), apparently there is a ''photostationary state'' for the fluctuations as well, provided the chemistry is fast enough. Unlike the first-order reaction where the fast chemistry limit implies $c' \to 0$, the chemical cycle allows nonvanishing fluctuations. If chemically induced fluctuations and turbulence induced fluctuations are not counteracting, it is conceivable that changing the reaction rate—and thus changing the relative strength of the processes—only results in small changes. It is worthwhile to take a closer look at the the chemical terms in the variance equations of the three species (5), which, to leading order, read

$$R_{\overline{a'^2}} = 2k\left[-A\overline{a'b'} - B\overline{a'a'} + \frac{j}{k}\overline{a'c'}\right], \quad (17)$$

$$R_{\overline{b'^2}} = 2k\left[-A\overline{b'b'} - B\overline{a'b'} + \frac{j}{k}\overline{b'c'}\right], \quad (18)$$

$$R_{\overline{c'^2}} = 2k\left[+A\overline{a'c'} + B\overline{a'a'} - \frac{j}{k}\overline{a'c'}\right]. \quad (19)$$

One may note that the chemical sources/sinks [(17)–(19)] in the variance equations vanish when (16) is satisfied. The variances of the three species can then develop comparable to the inert case. This leads to the following interpretation. At low Da, the chemical terms (17)–(19) are relatively small and the species behave roughly as inert species, but at large Da the net chemical terms appear to be small as well due to cancellation of various (large) terms. For moderate Da, some influence can be expected and is indeed observed in Fig. 5.

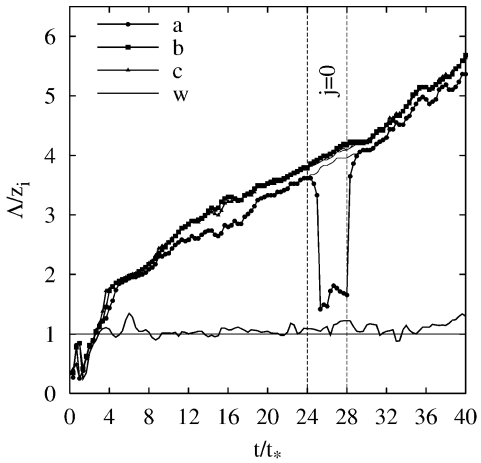

FIG. 6. The effect of a hypothetical passing cloud, which disturbs the chemical balance by affecting the photodissociation rate j. Until $t/t_* = 24$, the chemical system is in equilibrium. At this moment, the backreaction $c \xrightarrow{j} a + b$ is switched off ($j = 0$), bringing the chemistry out of balance. The backreaction is restored at $t/t_* = 28$. The variance dominating length scale Λ_a of the nonabundant species a experiences a dramatic decline but recovers comparably fast once the chemical cycle is closed again at $t/t_* = 28$. Note that Λ_b and Λ_c are nearly unaffected. Thin lines indicate the unperturbed case of Fig. 5.

For fast chemistry, Eq. (16) enforces a strong coupling between the fluctuations of the different species involved and it therefore entails a coupling between the turbulent fluxes, as can be seen by multiplication of (16) by w' and horizontally averaging:

$$A(z)\overline{w'b'}(z) + B(z)\overline{w'a'}(z) = \frac{j}{k}\overline{w'c'}(z). \quad (20)$$

This flux–profile relationship is indeed observed in the simulation for high Damköhler numbers (not shown), demonstrating that chemically induced fluctuations and turbulence-induced fluctuations can be compatible. Only very close to the surface, where the fluxes are prescribed and therefore not entirely compatible with (20), does one see deviations.

c. Chemistry out of equilibrium

The length scales in Fig. 5b exhibit hardly any dependence on the Damköhler number. The presence of a backreaction is essential for these results. A simple way to show the importance of the backreaction is by temporally switching it off, that is, by setting $j = 0$ for a while. Physically, one might envisage a passing cloud that blocks the incident solar radiation and therefore inhibits the backreaction $c \xrightarrow{j} a + b$, which results from photolysis. We simulated the effect of a hypothetical passing cloud by repeating the run with $k = 10^{-4}$ (ppb s)$^{-1}$ and $j = 10^{-3}$ s^{-1}, but with setting $j = 0$ from $t =$ 6 h ($=24t_*$) to $t = 7$ h ($=28t_*$). At $t = 7$ h the photodissociation rate j was set back to its original value $j = 10^{-3}$ s^{-1}.

In Fig. 6 we present the development of the variance

dominating scales of the species a, b, and c in time. One observes a rapid decline of Λ_a from $t = 24t_*$. This can be understood by considering again the equation for fluctuations (15). Because $j = 0$, and because species B is largely in excess, that is, $B \gg A$, the fluctuations a' due to chemistry are governed by

$$\frac{\partial}{\partial t}a' \simeq -kBa',$$

which is similar to the first-order reaction (14), with a corresponding Damköhler number of $\mathrm{Da} = kBt_* = 1.8$. In Fig. 2 we can read of a value of $\Lambda \approx 1.5$ at $\mathrm{Da} = 1.8$, in agreement with the value of Λ_a in Fig. 6 between $t/t_* = 24$ and 28.

One notices that the length scale of species b does not undergo a significant change; this can be understood as well. The fluctuation equation is equal to $\partial b'/\partial t \simeq -kBa'$. Because a and b are anticorrelated (a is a ''bottom-up'' and b is a ''top-down'' process), one finds for the chemical term (18) in the variance equation $R_{\overline{b'^2}} \simeq -2kB\overline{a'b'} > 0$. For the variance of species b, the chemical term therefore acts not as a sink, but as a source and is thus incapable of destroying large-scale variance.

Finally, when the cloud has passed at $t = 28t_*$ and the backreaction is set to its original value, Λ_a experiences a strong increase. In a relatively short time, Λ_a is back on its unperturbed value (thin line) and before long there is no hint of the perturbation anymore. The fast recovery (about one eddy turnover time) from $\Lambda_a = 1.5$ to 4 seems puzzling because in the initial course of the simulations it took about $25t_*$ to realize a similar increase (from $t = 4t_*$ to $29t_*$). How can the large-scale fluctuations of a suddenly grow that fast? Once the chemical equilibrium is restored, the fluctuations a' are directly fed by the mesoscale fluctuations in c, which are, at that time, *already present.* In the beginning of the simulation these mesoscale fluctuations were still developing.

5. A spectral model for describing length-scale evolution

The preceding sections revealed the effect of chemistry on spatial scales. To get more insight into the effect of chemical reactions on spatial scales, and in particular the (variance) dominating length scale, we will develop below an idealized spectral model of variance generation and consumption. Besides chemical sinks/sources and (spectral) production and dissipation of variance, the model must account for the interaction between wavenumbers—the ''cascade.'' We begin by deriving the model equation for the first-order reaction studied in section 3. Next we will generalize the model for the more complicated case of cyclic chemistry as studied in section 4.

a. Model derivation

The variance equation (7) in wavenumber space can be written (e.g., Stull 1988; Hinze 1972)

$$\frac{1}{2}\frac{d}{dt}E_c(\kappa) = -E_{wc}(\kappa)\frac{\partial C}{\partial z} - \frac{\partial T(\kappa)}{\partial z} - 4\pi^2 D_c \kappa^2 E_c(\kappa) - jE_c(\kappa) - S(\kappa), \quad (21)$$

where $E_c(\kappa)$ denotes the variance spectrum of c, and $E_{wc}(\kappa)$ is the cospectrum of w' and c'. The cospectrum $E_{wc}(\kappa)$ provides a spectral decomposition of the flux:

$$\overline{w'c'} = \int_0^\infty E_{wc}(\kappa)\, d\kappa, \quad (22)$$

which is analogous to (8). The precise definition of the spectra $E_c(\kappa)$ and cospectra $E_{wc}(\kappa)$, which are based on the two-dimensional Fourier transforms of c' and w', are given in appendix B. Note that the spectra still depend on height z and time t. In (21) we have also introduced $T(\kappa)$, which represents the spectral decomposition

$$\overline{w'c'^2} = \int_0^\infty T(\kappa)\, d\kappa. \quad (23)$$

The terms on the right-hand side of (21) can be identified as the spectral contributions to production, transport, dissipation, and chemistry. The last term on the right-hand side represents the net spectral transfer of variance in wavenumber space—the variance cascade. This term originates from the nonlinearity in the transport equation of c, which causes different wavenumbers to interact. Both $S(\kappa)$ and $\partial T(\kappa)/\partial z$ involve rather complicated expressions due to convolutions in Fourier space (e.g., Hinze 1972). It is important to note that the variance equation (7) can be retrieved from (21) by integrating over all wavenumbers; applying Eqs. (8), (22), and (23); and accounting for the fact that the net spectral transfer $S(\kappa)$ vanishes upon integration over the whole wavenumber range—$S(\kappa)$ only redistributes variance over the spectrum, but neither creates nor consumes variance.

We derive the vertically averaged version of (21) by integrating over z from 0 to z_i and dividing by z_i. Similar to the turbulent transport term in (7), the integrated transport term $\partial T(\kappa)/\partial z$ vanishes since no variance is transported across the boundaries. If we denote vertical averages by the angle brackets $\langle\ \rangle$, we obtain

$$\frac{1}{2}\frac{d}{dt}\langle E_c(\kappa)\rangle = P(\kappa) - S(\kappa) - D(\kappa) - R(\kappa). \quad (24)$$

The terms on the right-hand side represent spectral production of variance $P(\kappa)$, spectral transfer variance $S(\kappa)$, spectral dissipation of variance $D(\kappa)$, and the spectral source (sink) term due to chemistry $R(\kappa)$ and read

$$P(\kappa) = -\left\langle E_{wc}(\kappa)\frac{\partial C}{\partial z}\right\rangle, \qquad D(\kappa) = 4\pi^2 D_c \kappa^2 \langle E_c(\kappa)\rangle,$$
$$R(\kappa) = j\langle E_c(\kappa)\rangle. \tag{25}$$

In Eq. (24) both the production term $P(\kappa)$ and the spectral transfer term $S(\kappa)$ need to be modeled in order to obtain a closed set of equations. For notational convenience we work below with the shorthand notations $W(\kappa) = \langle E_w(\kappa)\rangle$ and $\Gamma(\kappa) = \langle E_c(\kappa)\rangle$. In order to model the spectral production, the cospectrum is expressed in terms of the spectra $W(\kappa)$ and $\Gamma(\kappa)$ and a spectral correlation coefficient $\alpha(\kappa)$: $\langle E_{wc}(\kappa)\rangle \simeq \alpha(\kappa)\sqrt{W(\kappa)\Gamma(\kappa)}$, where $\alpha(\kappa) \in [-1, 1]$. The spectral production can then be expressed as

$$P(\kappa) \simeq \alpha(\kappa)\sqrt{W(\kappa)\Gamma(\kappa)}\frac{c_*}{z_i}, \tag{26}$$

where c_* is the customary scalar fluctuation scale $c_* = |\varphi_c|/w_*$ with $\varphi_c \equiv \overline{w'c'}^s$ the surface flux. An analysis of the spectral correlation coefficients $\alpha(\kappa)$ in LES reveals a marginal dependence both on wavenumber and on the Damköhler number: $\alpha(\kappa) \simeq 0.7 \pm 0.1$. To reduce the complexity of the model we therefore proceed with a constant value: $\alpha(\kappa) = \alpha(=0.7)$.

Next, the net spectral transfer has to be modeled. On dimensional grounds, one can estimate its magnitude by

$$S(\kappa) \simeq \beta\Gamma(\kappa)\sqrt{\kappa^3 W(\kappa)}, \tag{27}$$

where β is a (positive) proportionality constant. Sophisticated models exist for spectral transfer (e.g., Batchelor 1953; Pao 1965; Leith 1967; Hinze 1972; Lesieur 1990), and in the next section we will indeed resort to one of these, but at this point it provides more conceptual insight by avoiding a complicated expression and using the magnitude estimate (27).

Inserting (26) and (27) together with $R(\kappa) = j\Gamma(\kappa)$ into (24), assuming stationarity, and focusing on large scales, which allows one to neglect the effect of dissipation, we arrive at the following balance:

$$\alpha\sqrt{W(\kappa)\Gamma(\kappa)}\frac{c_*}{z_i} \simeq \beta\sqrt{\kappa^3 W(\kappa)}\ \Gamma(\kappa) + j\Gamma(\kappa), \tag{28}$$

provided $\alpha > 0$. The parameters c_*, z_i, and j are given; β is a free parameter expressing the relative strength of the spectral spectral transfer. From (28) one can derive a closed expression for the species concentration variance spectrum

$$(\kappa) = \frac{c_*^2}{z_i^2}\frac{\alpha^2 W(\kappa)}{\left[\beta\sqrt{\kappa^3 W(\kappa)} + j\right]^2}. \tag{29}$$

Additional insight results from studying the dimensionless form; using $\tilde{\kappa} = \kappa z_i$, $\tilde{\Gamma} = \Gamma/z_i c_*^2$, $\tilde{W} = W/z_i w_*^2$ for the dimensionless wavenumber, dimensionless concentration spectrum, and dimensionless vertical velocity spectrum, respectively, we obtain

$$\tilde{\Gamma}(\tilde{\kappa}) = \frac{\alpha^2\tilde{W}(\tilde{\kappa})}{\left[\beta\sqrt{\tilde{\kappa}^3\tilde{W}(\tilde{\kappa})} + \mathrm{Da}\right]^2}. \tag{30}$$

The two extremes of a very small and very large Damköhler numbers are particularly interesting in (30). For fast chemistry $\mathrm{Da} \gg 1$, (30) simplifies to

$$\tilde{\Gamma}(\tilde{\kappa}) = \frac{\alpha^2}{\mathrm{Da}^2}\tilde{W}(\tilde{\kappa}). \tag{31}$$

The balance in (28) is then constituted solely by production and chemistry, rendering the contribution of spectral transfer insignificant. Equation (31) reveals that the spectra Γ and W becomes isomorphic, which entails that the dominant length scale of $\tilde{\Gamma}$ be equal to the dominant length scale of $\tilde{W}$. So $\Lambda_c/z_i = \Lambda_w/z_i \simeq 1$.

In the other limit, $\mathrm{Da} \to 0$, the balance in (28) is constituted by production and spectral transfer. One observes the peculiar fact that the vertical velocity spectrum then drops out in (30), yielding a spectrum independent of W:

$$\tilde{\Gamma}(\tilde{\kappa}) \sim \tilde{\kappa}^{-3}, \qquad \tilde{\kappa} \ll 1. \tag{32}$$

The interpretation is that the weak spectral production at large scales is balanced by spectral transfer, which in terms of W, is equally weak; that is, both scale with $\sqrt{W(\kappa)}$. But because spectral production scales with $\sqrt{\Gamma(\kappa)}$ and spectral transfer scales with $\kappa^{3/2}\tilde{\Gamma}$, the variance at large scales must become very large before spectral transfer is capable of balancing the production. This is expressed by (32), which also clearly implies that the variance dominating length scale is the largest scale resolved; that is, $\Lambda_c = L$ (lateral domain size).

In summary, the elementary spectral model (30) shows that the variance dominating length scale varies from mesoscales L for slow chemistry to the PBL height z_i for fast chemistry.

b. Advanced spectral transfer model

The magnitude estimate (27) for spectral transfer has some obvious limitations, because it cannot switch sign: a minimum condition on a spectral transfer model is that the net spectral transfer integrated over the whole wavenumber range be zero. Below we will consider the more sophisticated spectral transfer model proposed by Leith (1967), for which the generalization to scalars reads,

$$S(\kappa) = -\beta\frac{d}{d\kappa}\left\{\kappa^{13/2}\frac{d}{d\kappa}\left[\kappa^{-3}\sqrt{W(\kappa)}\Gamma(\kappa)\right]\right\}. \tag{33}$$

One may note that in the inertial subrange, when $W(\kappa) \sim \kappa^{-5/3}$ and $\Gamma(\kappa) \sim \kappa^{-5/3}$, the net spectral transfer vanishes: $S(\kappa) = 0$. Inserting (33) into (24) we find that in the stationary situation the variance spectrum $\Gamma(\kappa)$ satisfies

$$\underbrace{\alpha\sqrt{W(\kappa)\Gamma(\kappa)}\frac{c_*}{z_i}}_{P(\kappa)} = \underbrace{-\beta\frac{d}{d\kappa}\left\{\kappa^{13/2}\frac{d}{d\kappa}\left[\kappa^{-3}\sqrt{W(\kappa)}\Gamma(\kappa)\right]\right\}}_{S(\kappa)} + \underbrace{4\pi^2 D_c\kappa^2\Gamma(\kappa)}_{D(\kappa)} + \underbrace{j\Gamma(\kappa)}_{R(\kappa)}. \quad (34)$$

From this equation, one can numerically compute the variance spectrum $\Gamma(\kappa)$. As (34) is a second-order differential equation of the diffusion type, we employed the Gauss–Seidel algorithm in combination with (mild) successive overrelaxation (e.g., Press et al. 1992) to obtain a numerical solution for $\Gamma(\kappa)$. Rather than discretizing the problem in terms of the wavenumber κ, we introduced the variable $\xi = \log(\kappa)$ and discretized the problem uniformly in terms of ξ. We used 100 computational cells. Because the problem is only one-dimensional, it is quite affordable to encompass the full range of realistic scales, that is, to go from the mesoscale $L \sim 10^4$ m all the way down to the Kolmogorov scale ($\sim 10^{-3}$ m), allowing one to work with a realistic value of the diffusivity $D_c = 10^{-5}\,\mathrm{m^2\,s^{-1}}$. As mentioned above we use for α the empirical value of 0.7. Note that α only acts to globally rescale the spectrum: from (34) it follows that a different α' leads to $\Gamma_{\alpha'}(\kappa) = (\alpha'/\alpha)^2\,\Gamma_\alpha(\kappa)$.

As yet, Eq. (34) is not fully closed because of the presence of $W(\kappa)$. Rather than deriving a separate spectral model for $W(\kappa)$, which complicates matters considerably, we simply prescribe the velocity spectrum. Recall that the species concentration c has no effect on the dynamics. So treating the spectral properties of the dynamics simply as given, we study by (34) how the spectral properties $\Gamma(\kappa)$ depend on the effects of chemistry, that is, on the value of the Damköhler number Da. We prescribed the vertical velocity spectrum $W(\kappa)$ according to (e.g., Kaimal and Finnigan 1994):

$$W(\kappa) = [d_1(\kappa z_i)^{-\omega} + d_2(\kappa z_i)^{5/3}]^{-1}, \quad (35)$$

where ω, d_1, and d_2 are constants. The spectrum scales as $W(\kappa) \sim \kappa^{+\omega}$ for small wavenumbers ($\kappa z_i \ll 1$) and as $W(\kappa) \sim \kappa^{-5/3}$ for $\kappa z_i \gg 1$, with smooth behavior in between.

c. Results of first-order chemistry

For many values of j the variance spectrum $\Gamma(\kappa)$ was computed from (34). The scales, ranging from $L = 12.8$ km to 0.5 mm, were resolved using 100 computational cells uniformly distributed on $\log(\kappa)$. The diffusivity amounted to $D_c = 10^5\,\mathrm{m^2\,s^{-1}}$. Regarding the vertical velocity spectrum (35), good correspondence with the LES w spectrum was found in the large-scale range for the values $\omega = 3$, $d_1 = 1.2 \times 10^{-4}$, $d_2 = 0.01$. We used the same values for z_i and w_* as in the LES; that is, $z_i = 800$ m and $w_* = 0.86\,\mathrm{m\,s^{-1}}$; from $\varphi_c = 0.1$ ppb m $\mathrm{s^{-1}}$, one obtains $c_* \equiv |\varphi_c|/w_* \approx 0.12$ ppb. The model constant β, controlling the overall strength of spectral transfer, was set to unity.

In Fig. 7 the resulting spectra and dominating length scales have been presented for various Damköhler numbers. Figure 7b shows the computed spectra on the full-scale range and reveals the inertial subrange behavior from roughly 100 m to 1 cm (4 decades). Since the total variance is determined by the large scales of the spectrum, and because it facilitates comparison with the LES spectra of Fig. 1, we plotted the spectra also on the LES scale range in Fig. 7a. One may observe a fair agreement. In particular the ''double mode'' structure of the spectra for $\mathrm{Da} < 1$ is interesting. For $\mathrm{Da} = 10^{-2}$ the spectral model predicts even more variance on mesoscales than LES does, but this can be explained by the fact that LES spectrum has not equilibrated yet (see Fig. 2a). In Fig. 7c, the variance dominating length scale based on the location of the spectral peak $\Lambda = 1/\kappa_{\mathrm{peak}}$ has been presented as a function of the Damköhler number. Comparing with the LES results of Fig. 2b, one observes a good agreement: large values of Λ for small values of Da and $\Lambda/z_i \approx 1$ for large Da, with the transition near $\mathrm{Da} = 1$. The steepness of the transition is a result of the double mode of the spectra: instead of merging, the modes remain distinct, and at $\mathrm{Da} \approx 1$ the second mode takes over, leading to a jump in the peak wavenumber. For small Damköhler numbers the spectral model yields larger values for Λ than LES, which is due to the fact that the LES length scales are still growing for $\mathrm{Da} \leq 10^{-1}$ (see Fig. 2a).

It is interesting to study in more detail the various contributions to the spectral variance budget (34). These contirbutions, spectral production $P(\kappa)$, spectral transfer $S(\kappa)$, dissipation $D(\kappa)$, and consumption of variance due to chemistry $R(\kappa)$, respectively, are depicted in Fig. 8 for three cases: $\mathrm{Da} \ll 1$, $\mathrm{Da} = 1$, and $\mathrm{Da} \gg 1$. The data are presented in conservative form, that is, multiplied by κ to account for the logarithmic κ axis and normalized by the maximum of the production term.

For small Damköhler numbers (Fig. 8, top), the major balance is constituted between spectral production and spectral transfer; the spectral transfer removes the variance from the scales where it is produced (large scales) and transports it to small scales where it is dissipated. The chemical term plays no significant role in the budget. Conversely, in the fast chemistry or high Damköhler number limit (Fig. 8, bottom), dissipation has become unimportant. The major balance is between production by turbulence, on the one hand, and consumption by chemistry, on the other. Because, unlike dissipation, the chemical consumption process is equally effective on all scales, spectral transfer plays no role either. The chemical term directly consumes the variance at the scale where it is produced. The case $\mathrm{Da} = 1$ is clearly intermediate between these two limits.

The spectral model (34) enables one to study the theoretical behavior on very large scales—theoretical, be-

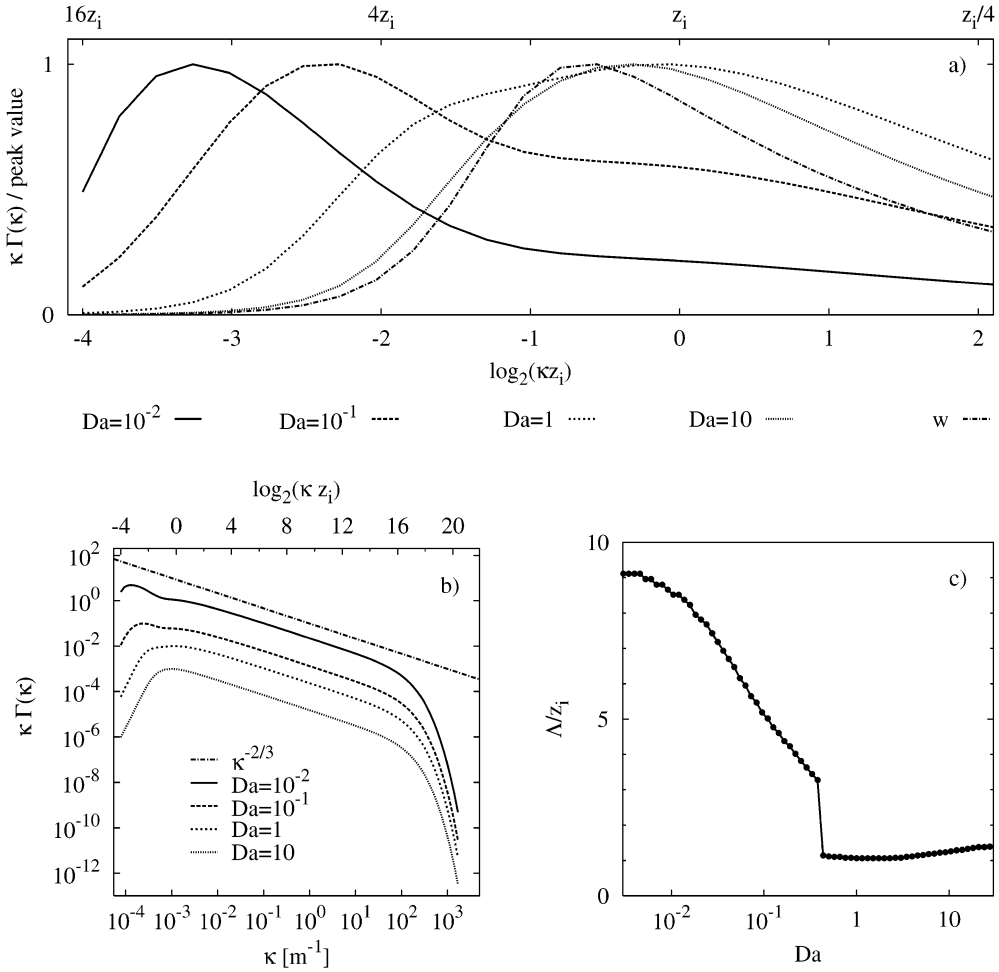

FIG. 7. (a) Variance spectra $\Gamma(\kappa)$ numerically computed from (34) for various Damköhler numbers. The spectra have been plotted on the same scale range as the LES spectra in Fig. 1 to facilitate comparison. They have been additionally normalized by the peak value of the spectra. (b) The same spectra as in (a) but plotted on the full scale range and on a double logarithmic scale (with an arbitrary offset between the graphs) to reveal the inertial subrange scaling $\kappa\Gamma(\kappa) \sim \kappa^{-2/3}$, (c) The variance dominating length scale Λ of a first order reacting species as a function of the Damköhler number, as predicted by the spectral model (cf. Fig. 2b).

cause no additional large-scale forcings are taken into account. So just for the sake of the principle, we set $L = 10^3$ km, leaving the remaining parameters unaltered. We briefly summarize the results. 1) In the inert case (Da = 0), one clearly observes $\Gamma(\kappa) \sim \kappa^3$ for $\kappa z_i \ll 1$, consistent with (32). 2) For Da $\ll 1$ (but nonzero), one finds $\Lambda \sim \mathrm{Da}^{-1/3}$.

These results can be understood as follows. 1) Indeed, at large scales $W(\kappa) \sim \kappa^\omega$ so that $\Gamma(\kappa) \sim \kappa^{-3}$ is a solution to (34) when Da = 0. 2) Because the dominating length scale is determined by the large-scale range, Eq. (30) with $W(\kappa) \sim \kappa^\omega$ can provide insight. Differentiation of (30) with respect to $\tilde{\kappa}$ and equating to zero yields the equation that determines the peak wavelength: $\tilde{\kappa}_{\mathrm{peak}} \sim \mathrm{Da}^{2/(3+\omega)}$. Hence, the dominating length scale is $\Lambda/z_i \sim \mathrm{Da}^{-2/(3+\omega)}$, consistent with result 2, because $\omega = 3$. Unfortunately, it will be very hard to verify predictions 1 and 2 with LES not only because of the required magnitude of the lateral domain size, but also because of the enormous simulation time to reach a steady state.

d. Binary chemistry with a backreaction

Finally, we applied the spectral model to the more complicated case of chemistry in a cycle as studied in section 4. To this end we derived evolution equations for the spectra of the different species in the same manner as outlined in section 5b. Production, spectral transfer, and dissipation are treated analogously, but the spectral representations of the chemical terms (17) through (19) are somewhat more involved as they contain cospectra. We model these according to $E_{ab}(\kappa) = \rho_{ab}\sqrt{E_a(\kappa)E_b(\kappa)}$, where ρ_{ab} denotes the (average) spectral correlation. The governing equations for the spectra then read

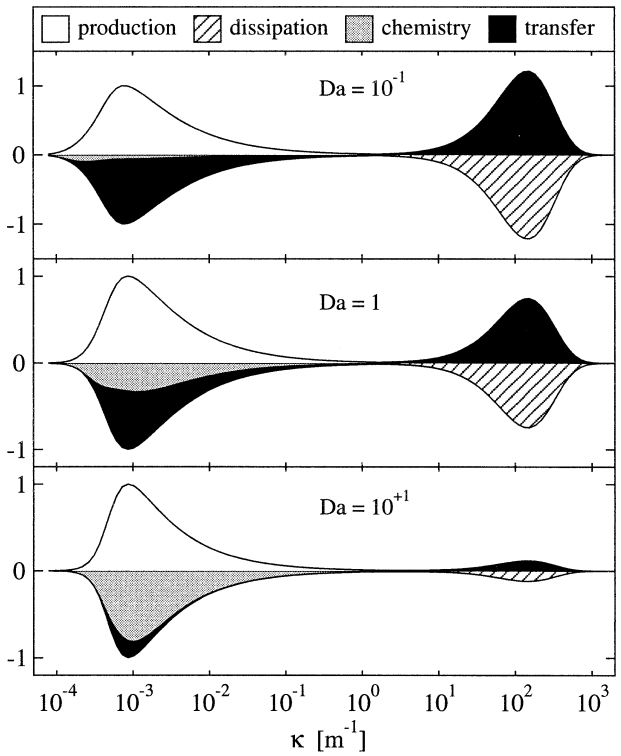

FIG. 8. Spectral contributions appearing in the variance budget equation (34) multiplied by the wavenumber κ, that is, production $\kappa P(\kappa)$, transfer $\kappa S(\kappa)$, dissipation $\kappa D(\kappa)$, and chemistry $\kappa R(\kappa)$. The results are presented for three chemical regimes: Da $\ll 1$ (slow chemistry), Da $= 1$ (intermediate), and Da $\gg 1$ (fast chemistry). The scale range covers 7 orders of magnitude (10^4 m to less than 10^{-3} m). For Da $= 10^{-1}$ variance is produced at large scales, then transported to small scales by spectral transfer, where dissipation takes place. Chemistry plays an insignificant role. For Da $= 10^{+1}$ turbulence still produces variance at relatively large scales, but this is directly consumed by the action of chemistry. Spectral transfer and dissipation play a minor role. Here Da $= 1$ is clearly intermediate.

$$\frac{1}{2}\frac{d}{dt}E_a(\kappa) = P_a(\kappa) - S_a(\kappa) - D_a(\kappa) - kA\rho_{ab}\sqrt{E_aE_b} - kBE_a + j\rho_{ac}\sqrt{E_aE_c}, \quad (36)$$

$$\frac{1}{2}\frac{d}{dt}E_b(\kappa) = P_b(\kappa) - S_b(\kappa) - D_b(\kappa) - kAE_b - kB\rho_{ab}\sqrt{E_aE_b} + j\rho_{bc}\sqrt{E_bE_c}, \quad (37)$$

$$\frac{1}{2}\frac{d}{dt}E_c(\kappa) = P_c(\kappa) - S_c(\kappa) - D_c(\kappa) + kA\rho_{bc}\sqrt{E_bE_c} + kB\rho_{ac}\sqrt{E_aE_c} - jE_c, \quad (38)$$

where, for $d = a, b, c$, $P_d(\kappa) = \rho_{wd}\sqrt{W(\kappa)E_d(\kappa)}d_*/z_i$ and $D_d(\kappa) = 4\pi^2 D_d\kappa^2 E_d(\kappa)$; S_d is given by (33) with $\Gamma(\kappa)$ replaced by $E_d(\kappa)$. Because, in the present case, a and c are premixed, in contrast to b, we use $\rho_{ac} = 1$, $\rho_{ac} = \rho_{bc} = -1$. We took $\rho_{wa} = \rho_{wb} = \rho_{wc} = 0.7$ as before. Setting $d/dt \to 0$, we numerically computed the spectra from (36)–(38) using the same method as described for first-order chemistry. From the resulting spectra, the dominating length scales Λ_a, Λ_b, Λ_c were derived. In Fig. 9 these are plotted as a function of the Damköhler number defined in (13). The spectral model predicts only a weak dependence on the Damköhler number in good agreement with the LES results shown in Fig. 5b. On the whole, the length scales are slightly larger, because the LES results were not fully equilibrated (Fig. 5a), but the shape of the curves in Fig. 9 clearly resembles those of Fig. 5b.

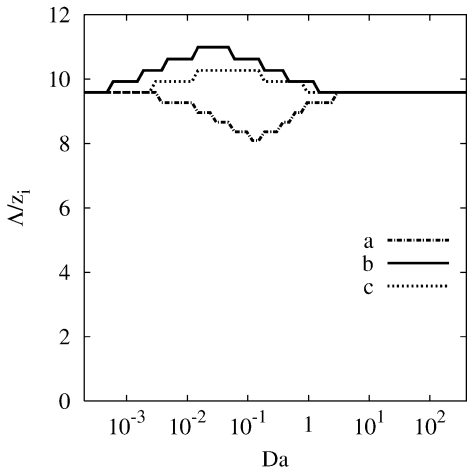

FIG. 9. Predictions by the spectral model (36)–(38) of the variance dominating length scales of the three species involved in the chemical reaction (1), (2) for various Damköhler numbers (cf. with Fig. 5b).

6. Conclusions

The impact of reaction rate and reaction type on the variance spectra of chemical species has been studied. To this end large-eddy simulations of the dry convective boundary layer were conducted with a relatively large domain size in order to accommodate the potential development of mesoscale fluctuations. From the variance spectra of the reactants, a variance dominating length scale was derived, which is representative of the horizontal length scale that contributes most to the total variance of a variable.

For a first-order reaction, a clear dependence was observed between the dominating length scale of the species and the reaction rate. For small Damköhler numbers (slow chemistry) mesoscale fluctuations would slowly but gradually dominate the variance, in concord with the findings of Jonker et al. (1999) for inert species in a CBL. For large Damköhler numbers mesoscale fluctuations did not develop, and the mixed-layer depth emerged as the variance dominating scale.

For a binary reaction mechanism endowed with a backreaction, the impact of the overall reaction rate was rather weak. Unlike the first-order reaction, a chemical balance is reached. In this equilibrium state, chemically induced fluctuations and turbulence fluctuations turn out to be mutually compatible. Changing the reaction rate,

and therefore changing the relative strength of the processes, then induces only small effects. However, when the chemical equilibrium was perturbed by temporarily switching off the backreaction, a collapse of the variance dominating scale of the least abundant species was observed. Restoring the backreaction entailed an equally fast recovery of the large-scale fluctuations. This kind of behavior reveals the susceptibility of the chemical system to external perturbations. Disturbances like sudden local surface emissions, or passing clouds that affect photochemistry, etc., perturb the chemical equilibrium and clearly have a big impact on the variability.

Finally, we developed a spectral model to shed more light on the mechanism along which chemistry influences length scales. The model encompassed a huge range of scales, from mesoscales down to the Kolmogorov scale; incorporated spectral production of variance by turbulence, spectral dissipation of variance, chemical sinks/sources; and accounted for the interaction between scales. The model results turn out to be in good agreement with the LES results: the shape of the predicted spectra, the location of the spectral peak, as well as the dependence on the Damköhler number could be reproduced quite accurately. For the second-order reaction with backreaction, the model predicts a weak dependence on the Damköhler number, also in agreement with the LES results.

In general we find that the characteristic length scales of reactive species depend on the reaction rate and the reaction type. This could be relevant for the definition of a master length scale used in the parameterization of turbulent fluxes in large-scale atmospheric chemistry models.

Acknowledgments. Two authors (HJ and JVGA) acknowledge the NATO collaborative research Grant CRG 970040 to sponsor their respective research visits. We would like to thank Dr. Maarten Krol for many discussions. Three anonymous reviewers are gratefully acknowledged for their critical remarks and useful suggestions. This work was sponsored by the National Computing Facilities Foundation (NCF) for the use of supercomputer facilities, with financial support of NWO.

APPENDIX A

Analytical Solution of the Chemical System

The chemical solver used in the LES model is based on the analytical solution of the reaction system (1) and (2). The nonlinear equation system can be written

$$\frac{\partial a}{\partial t} = -kab + jc, \tag{A1}$$

$$\frac{\partial b}{\partial t} = -kab + jc, \tag{A2}$$

$$\frac{\partial c}{\partial t} = +kab - jc, \tag{A3}$$

where the initial concentrations at $t = 0$ are a_0, b_0, and c_0. This system can be solved analytically to give the following expression for the concentration of reactant a:

$$a(t) = \frac{a_\infty(a_0 - b_\infty)(1 - e^{-kDt}) + a_0(a_\infty - b_\infty)e^{-kDt}}{(a_0 - b_\infty)(1 - e^{-kDt}) + (a_\infty - b_\infty)e^{-kDt}}, \tag{A4}$$

where the discriminant D is the *positive* root:

$$D = \sqrt{(a_0 - b_0)^2 + \lambda^2 + 2\lambda(a_0 + b_0 + 2c_0)},$$

which is always real. The equilibrium values a_∞ and b_∞, expressed as functions of the initial concentrations and the ratio $\lambda = j/k$, are

$$a_\infty = \frac{1}{2}(a_0 - b_0 - \lambda + D),$$

$$b_\infty = \frac{1}{2}(a_0 - b_0 - \lambda - D).$$

The solutions for b and c are

$$b(t) = b_0 + a(t) - a_0, \tag{A5}$$

$$c(t) = c_0 - a(t) + a_0. \tag{A6}$$

Equation (A4) reduces for $\lambda = 0$ to the solution found by Corrsin (1968) for a second-order irreversible reaction $a + b \xrightarrow{k} c$. With, for example, $a_0 > b_0$:

$$a_\infty = \frac{1}{2}(a_0 - b_0 + |a_0 - b_0|) = a_0 - b_0, \tag{A7}$$

$$b_\infty = \frac{1}{2}(a_0 - b_0 - |a_0 - b_0|) = 0, \tag{A8}$$

hence (A4) becomes

$$\frac{a(t)}{a_0} = \frac{[1 - a_0/b_0]\exp\{-k(b_0 - a_0)t\}}{1 - (a_0/b_0)\exp\{-k(b_0 - a_0)t\}}. \tag{A9}$$

The chemical time scale τ of the system (A1)–(A3) can be extracted from the exponential in (A4) by equating $\exp[k(b_\infty - a_\infty)t] \equiv \exp(-t/\tau)$, which yields $\tau = 1/kD$, or

$$\tau = \frac{1}{\sqrt{k^2(a_0 - b_0)^2 + j^2 + 2jk(a_0 + b_0 + 2c_0)}}. \tag{A10}$$

If species b is largely in excess, $b_0 \approx B \gg a_0$, c_0, this expression reduces to $\tau \approx 1/(kB + j)$.

APPENDIX B

Spectral Densities

Variables are decomposed into a mean and fluctuating part:

$$a(x, y, z, t) = \overline{a}(z, t) + a'(x, y, z, t),$$

$$\overline{a}(z, t) \equiv \frac{1}{L^2}\iint a(x, y, z, t)\, dx\, dy,$$

where L denotes the horizontal domain size. We will confine ourselves to situations where $L_x = L_y = L$ and grid spacing $\Delta x = \Delta y = \Delta$. The two-dimensional Fourier transform of a' into the wavenumbers $\mathbf{k} = (k_x, k_y)$ is

$$\hat{a}(\mathbf{k}) \equiv \int\int \exp[2\pi i(k_x x + k_y y)]a'(x, y, z, t)\, dx\, dy,$$

where it is understood that $\hat{a}(\mathbf{k})$ still has a height and time dependence; that is, $\hat{a}(\mathbf{k}) = \hat{a}(\mathbf{k}, z, t)$. By virtue of Parseval's identity, (co)variances can be decomposed into contribution per wave vector according to

$$\overline{a'b'} = \frac{1}{L^2}\int\int a'(x, y, z, t)b'(x, y, z, t)\, dx\, dy = \frac{1}{2}\int\int [\hat{a}(\mathbf{k})\hat{b}^*(\mathbf{k}) + \hat{a}^*(\mathbf{k})\hat{b}(\mathbf{k})]\, d\mathbf{k}. \quad \text{(B1)}$$

Due to symmetry considerations, one knows that all variables will obey horizontal isotropy, which is why it is favorable to express the spectral density in terms of the length of the wave vector $\mathbf{k}$:

$$\overline{a'b'} = \int_0^\infty E_{ab}(k)\, dk. \quad \text{(B2)}$$

The density $E_{ab}(k)$ represents the cospectrum of a and b. It is related to the Fourier transforms of a' and b' by

$$E_{ab}(k) = \frac{1}{2}\int\int [\hat{a}(\mathbf{k})\hat{b}^*(\mathbf{k}) + \hat{a}^*(\mathbf{k})\hat{b}(\mathbf{k})] \times \delta(|\mathbf{k}| - k)\, d\mathbf{k}, \quad \text{(B3)}$$

where δ denotes the well-known Dirac function. The validity of the decomposition (B2) is readily verified by substituting (B3) in (B2), carrying out the integral over k, and subsequently using (B1).

Note that both $\overline{a'b'} = \overline{a'b'}(z, t)$ and $E_{ab}(k) = E_{ab}(k, z, t)$, but we will omit to indicate so for notational convenience. Note also that, in any practical situation, the spectral density $E_{ab}(k)$ does not extend over the whole $[0, \infty\rangle$ as indicated by (B2). The wavenumber range for k_x and k_y is confined by domain size and resolution, or rather the Nyquist ''frequency'' $1/(2\Delta x)$. For this reason the density $E_{ab}(k)$ vanishes outside the range $k \in [1/L, \sqrt{2}/(2\Delta x)]$.

For variance spectra we can simply put $b' = a'$ in Eqs. (B1)–(B3):

$$\overline{a'^2} = \int_0^\infty E_a(k)\, dk, \quad \text{(B4)}$$

where

$$E_a(k) \equiv \int\int |\hat{a}(\mathbf{k})|^2\delta(|\mathbf{k}| - k)\, d\mathbf{k}. \quad \text{(B5)}$$

Another way of writing (B5) is

$$E_a(k) \equiv \int_{-\pi}^{\pi} k|\hat{a}(k, \phi)|^2\, d\phi,$$

which results from switching to polar coordinates $\mathbf{k} = (|\mathbf{k}|\cos\phi, |\mathbf{k}|\sin\phi)$. For the cospectrum, a similar equation holds.

REFERENCES

Batchelor, G. K., 1953: *The Theory of Homogeneous Turbulence.* Cambridge University Press, 197 pp.

Brown, R. J., and R. W. Bilger, 1996: An experimental study of a reactive plume in grid turbulence. *J. Fluid Mech.*, **312,** 373–407.

Calvert, J., and W. Stockwell, 1983: Deviations from the $O_3 - NO - NO_2$ photostationary state in troposphere chemistry low order models representing realizations of turbulence. *Can. J. Chem.*, **61,** 983–992.

Corrsin, S., 1961: The reactant concentration spectrum in turbulent mixing with a first-order reaction. *J. Fluid Mech.*, **11,** 407–416.

——, 1968: Effect of passive chemical reaction on turbulents dispersion. *AIAA J.*, **6,** 1797–1798.

Cuijpers, J. W. M., and P. G. Duynkerke, 1993: Large eddy simulations of trade wind with cumulus clouds. *J. Atmos. Sci.*, **50,** 3894–3908.

de Roode, S. R., P. G. Duynkerke, and H. J. J. Jonker, 2004: Large-eddy simulation: How large is large enough? *J. Atmos. Sci.*, in press.

Delany, A., D. Fitzjarrald, D. Lenschow, R. Pearson Jr., G. Wendeland, and B. Woodruff, 1986: Direct measurements of nitrogen oxides and ozone fluxes over grassland. *J. Atmos. Chem.*, **4,** 429–444.

Dörnbrack, A., 1997: Broadening of convective cells. *Quart. J. Roy. Meteor. Soc.*, **123,** 829–847.

Feijt, A., and H. J. J. Jonker, 2000: Comparison of scaling parameters from spatial and temporal distributions of cloud properties. *J. Geophys. Res.*, **105,** 29 089–29 097.

Fiedler, B. H., 1993: Cell broadening in three-dimensional thermal convection between poorly conducting boundaries. *Beitr. Phys. Atmosph.*, **66,** 173–181.

——, and M. Khairoutdinov, 1994: Cell broadening in three-dimensional thermal convection between poorly conducting boundaries: Large eddy simulations. *Beitr. Phys. Atmos.*, **67,** 235–241.

Galmarini, S., and P. Thunis, 2000: Estimating the contribution of Leonard and cross terms to the subfilter scale from atmospheric data. *J. Atmos. Sci.*, **57,** 1785–1796.

——, F. Michelutti, and P. Thunis, 1999: Evaluation of Leonard and cross terms from atmospheric data. Preprints, *13th Symp. Boundary Layer Turbulence,* Dallas, TX, Amer. Meteor. Soc., 115–118.

Gao, W., and M. L. Wesely, 1994: Numerical modelling of the turbulent fluxes of chemically reactive trace gases in the atmospheric boundary layer. *J. Appl. Meteor.*, **33,** 835–847.

Garratt, J. R., 1992: *The Atmospheric Boundary Layer*. Cambridge University Press, 316 pp.

Hinze, J. O., 1972: *Turbulence.* McGraw-Hill, 790 pp.

Jonker, H. J. J., P. Duynkerke, and J. W. M. Cuijpers, 1999: Mesoscale fluctuations in scalars generated by boundary layer convection. *J. Atmos. Sci.*, **56,** 801–808.

Kaimal, J., and J. Finnigan, 1994: *Atmospheric Boundary Layer Flows, Their Structure and Measurements.* Oxford University Press, Oxford, 289 pp.

Krol, M. C., M. J. Molemaker, and J. Vilà-Guerau de Arellano, 2000: Effects of turbulence and heterogeneous emissions on photochemically active species in the convective boundary layer. *J. Geophys. Res.*, **105,** 6871–6884.

Leith, C., 1967: Diffusion approximation to inertial energy transfer in isotropic turbulence. *Phys. Fluids,* **10,** 1409–1416.

Lenschow, D. H., A. C. Delany, B. B. Stankov, and D. H. Stedman, 1980: Airborne measurements of the vertical flux in the boundary layer. *Bound.-Layer Meteor.,* **19,** 249–265.

Lesieur, M., 1990: *Turbulence in Fluids.* Kluwer, 412 pp.

Lewellen, D. C., and W. Lewellen, 2001: Effects of aircraft wake dynamics on measured and simulated NO_x and HO_x wake chemistry. *J. Geophys. Res.*, **106,** 27 661–27 672.

Madronich, S., 1987: Photodissociation in the atmosphere: 1. Actinic fluxes and the effects of ground reflections and clouds. *J. Geophys. Res.,* **92,** 9740–9752.

Müller, G., and A. Chlond, 1996: Three-dimensional numerical study of cell broadening during cold-air outbreaks. *Bound.-Layer Meteor.,* **81,** 289–323.

Nucciarone, J. J., and G. S. Young, 1991: Aircraft measurements of turbulence spectra in the marine stratocumulus-topped boundary layer. *J. Atmos. Sci.,* **48,** 2382–2392.

Pao, Y.-H., 1965: Structure of turbulent velocity and scalar fields at large wavenumbers. *Phys. Fluids,* **8,** 1063–1075.

Patton, E. G., K. J. Davis, M. C. Barth, and P. Sullivan, 2001: Decaying scalars by forest canopy: A numerical study. *Bound.-Layer Meteor.,* **100,** 91–129.

Pearson R., Jr., S. Oncley, and A. Delany, 1998: A scalar similarity study based on surface layer ozone measurements over cotton during California ozone deposition experiment. *J. Geophys. Res.,* **103,** 18 919–18 926.

Press, W., S. Teukolsky, W. Vetterling, and B. Flannery, 1992: *Numerical Recipes in C: The Art of Scientific Computing.* Cambridge University Press, 994 pp.

Schumann, U., 1989: Large-eddy simulation of turbulent diffusion with chemical reactions in the convective boundary layer. *Atmos. Environ.,* **23,** 1713–1729.

Shao, Q., and D. A. Randall, 1996: Closed mesoscale cellular convection driven by cloud-top radiative cooling. *J. Atmos. Sci.,* **53,** 2144–2165.

Stull, R. B., 1988: *An Introduction to Boundary Layer Meteorology.* Kluwer, 666 pp.

Sykes, R. I., D. S. Henn, and S. F. Parker, 1992: Large-eddy simulation of a turbulent reacting plume. *Atmos. Environ.,* **26A,** 2565–2574.

Vilà-Guerau de Arellano, J., J. Talmon, and P. J. H. Builtjes, 1990: A chemically reactive plume model for the NO–NO_2–O_3 system. *Atmos. Environ.,* **24A,** 2237–2246.

Vinuesa, J. F. ,and J. Vilà-Guerau de Arellano, 2003: Fluxes and (co-)variances of reacting scalars in a convective atmospheric boundary layer. *Tellus-B,* **55,** 935–949.

Vreugdenhil, C. B., and B. Koren, 1993: *Notes on Numerical Fluid Mechanics. Numerical Methods for Advection–Diffusion.* Vieweg, 373 pp.

Young, G., 1987: Mixed layer spectra from aircraft measurements. *J. Atmos. Sci.,* **44,** 1251–1256.